

Observation-Graph Interaction and Key-Detail Guidance for Vision and Language Navigation

Yifan Xie^{1,2}, Binkai Ou³, Fei Ma⁴, and Yaohua Liu^{2†}

Abstract—Vision and Language Navigation (VLN) requires an agent to navigate through environments following natural language instructions. However, existing methods often struggle with effectively integrating visual observations and instruction details during navigation, leading to suboptimal path planning and limited success rates. In this paper, we propose OIKG (Observation-graph Interaction and Key-detail Guidance), a novel framework that addresses these limitations through two key components: (1) an observation-graph interaction module that decouples angular and visual information while strengthening edge representations in the navigation space, and (2) a key-detail guidance module that dynamically extracts and utilizes fine-grained location and object information from instructions. By enabling more precise cross-modal alignment and dynamic instruction interpretation, our approach significantly improves the agent’s ability to follow complex navigation instructions. Extensive experiments on the R2R and RxR datasets demonstrate that OIKG achieves state-of-the-art performance across multiple evaluation metrics, validating the effectiveness of our method in enhancing navigation precision through better observation-instruction alignment.

I. INTRODUCTION

Vision and Language Navigation (VLN) [1] is a challenging task that requires an AI agent to navigate through complex 3D environments [2], [3] by following natural language instructions. In this task, agents must process visual information from their surroundings while interpreting detailed navigation instructions to reach specified target locations. This involves understanding spatial relationships, recognizing objects and landmarks, and making sequential navigation decisions based on the cross-modal alignment between visual observations and linguistic guidance.

Recent methods [4]–[9] have shown promising results by incorporating topological maps to enhance navigation decision-making. Rather than simply predicting step-by-step actions like “turn left” or “go forward”, these methods build a graph representation that records all previously visited viewpoints and their connections. This graph-based memory allows the agent to make strategic navigation decisions across its entire explored environment. Using these topological maps, the agent processes spatial and linguistic information through Graph Convolutional Networks (GCNs), where each node in the graph represents a viewpoint and updates its features by aggregating information from connected locations. This process enables more effective long-range navigation planning compared to purely local decision-making. DUET [4] combines coarse-scale global encoding

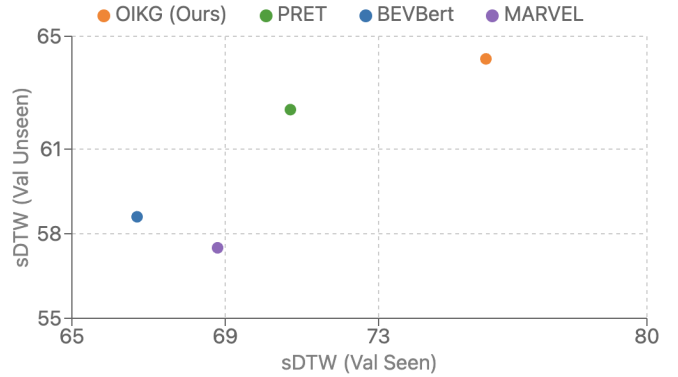


Fig. 1. Comparison of sDTW on the RxR val seen split and the RxR val unseen split. OIKG demonstrates the ability to achieve optimal sDTW across various splits.

of a topological map with fine-scale local encoding of the current node for navigation decisions. BEVBert [8] proposes a novel map-based pre-training framework that combines local metric maps for short-term spatial reasoning with global topological maps for long-term planning, introducing an innovative hybrid mapping approach to enhance language-guided navigation through better spatial-aware cross-modal reasoning. PRET [9] plans navigation by aligning language instructions with directed fidelity trajectories, using orientation-aware features in a directed graph representation instead of traditional GCN-based map encoding.

Despite significant progress in VLN research, existing methods face several key limitations. Current methods often struggle to effectively integrate visual observations [10], [11] with instruction details [12], [13] during navigation, leading to suboptimal path planning and limited success rates. Many approaches process visual and angular information together without considering their distinct characteristics, potentially causing interference in feature representation. Additionally, existing methods typically treat instructions as a whole through simple attention mechanisms, lacking the ability to extract and utilize fine-grained navigational cues effectively.

In this paper, we propose OIKG (Observation-graph Interaction and Key-detail Guidance), a novel framework that addresses the limitations of existing VLN methods through two key components. First, our observation-graph interaction module decouples angular and visual information while strengthening edge representations in the navigation space through geometric embedding. This decoupling approach enables more effective processing of spatial information by mitigating interference between different feature types,

[†]Corresponding author. (Corresponding email: liuyaohua@gdiist.cn)

¹ Xi’an Jiaotong University ² Guangdong Institute of Intelligence Science and Technology ³BoardWare Information System Company Ltd ⁴Guangdong Laboratory of Artificial Intelligence and Digital Economy (SZ)

and the enhanced edge representation helps the agent better understand spatial relationships in the navigation environment. Second, we introduce a key-detail guidance module that dynamically extracts and utilizes fine-grained location and object information from instructions. Unlike existing methods that process instructions as a whole through simple attention mechanisms, our module allows for more precise cross-modal alignment between visual observations and textual guidance by separately considering location details (like "bedroom", "doorway") and object details (like "table", "window"). Our method enables the agent to better understand and follow complex navigation instructions while maintaining awareness of critical environmental details. Through the combination of these two innovative components, OIKG achieves more effective integration of visual observations and instruction details during navigation, leading to improved path planning and higher success rates compared to existing approaches. To evaluate the performance of our proposed OIKG, we conduct experiments on the R2R and RxR datasets. The experimental results demonstrate that the proposed OIKG can achieve superior performance. Fig. 1 demonstrates that our method achieves the best sDTW compared to other methods in different settings.

Our contributions can be summarized as follows:

- We propose a novel vision and language navigation method, named OIKG, which combines observation-graph interaction and key-detail guidance for more precise navigation planning and instruction following.
- We introduce the observation-graph interaction module to decouple angular and visual information while strengthening edge representation through geometric embedding in the navigation space.
- We design the key-detail guidance module to dynamically extract and utilize fine-grained location and object information from instructions for better cross-modal alignment.

II. RELATED WORK

A. Vision and Language Navigation

In recent years, Vision and Language Navigation (VLN) has emerged as a prominent research direction [4]–[9], [14]–[16]. The initial approaches to VLN employed LSTM-based sequence-to-sequence architectures to map natural language instructions to either atomic actions or waypoint-level decisions, operating on discretized 360-degree panoramic views of the environment.

SpeakerFollower [14] pioneers the use of back-translation in VLN, addressing the limited availability of training data. EnvDrop [17] introduces environment augmentation through feature-level dropout to combat visual input overfitting. This innovation sparks numerous environment augmentation methods [18], [19] in the field. Different attention mechanisms [20]–[22] are also introduced to enhance cross-modal alignment between visual and textual inputs. PREVALENT [23] introduces a pioneering approach by pretraining

transformer encoders on VLN datasets. MTVM [24] explores the navigation history memorization and employs transformer architecture to develop robust planning strategies.

Additionally, navigation strategy plays a crucial role in VLN, as agents must effectively navigate in unseen environments, requiring exploration and environmental familiarization. DUET [4] implements a dual-scale transformer architecture for making both local and global predictions. AZHP [5] introduces hierarchical graph structures to enhance exploration capabilities. Meta-Explore [6] incorporates a dedicated module to explicitly determine backtracking decisions. BEVBert [8] integrates both local metric maps and global topological maps to strengthen spatial understanding in language-guided navigation. PRET [9] aligns language instructions with trajectory features within a directed graph structure, implementing orientation-aware path planning as an alternative to conventional map encoding methods. In our method, we utilize the directed graph structure and introduce the observation-graph interaction to strengthen the edge representation.

B. Maps for Navigation

Maps for navigation have been a fundamental component in visual navigation research, with a long evolution from SLAM-based approaches [25], [26] to more sophisticated representations [27], [28]. Initially, research focused on using SLAM to construct metric maps for planning [29], providing precise spatial layouts but facing computational efficiency challenges due to their grid-based nature. To address these limitations, several methods [30], [31] adopted topological graphs for global planning, offering a more efficient but coarse-grained representation. The field then progressed to hybrid approaches that combine the strengths of both representations - metric maps provide detailed local spatial information while topological maps enable efficient long-term planning. Recent works [4], [8], [32] have introduced learnable hybrid topological and metric maps, such as BEVBert [8] that balances representation ability with computational cost. However, the computational demands of processing these hybrid maps remain significant. Other works [9], [31] explore novel process involving directed topo-maps with trajectory-based planning, which allows for incremental embedding calculations and reduces overall computational costs while maintaining effective navigation capabilities. These evolving mapping methods reflect the ongoing effort to balance the trade-off between precise spatial representation and computational efficiency in visual navigation systems.

III. METHOD

A. Problem Statement

Vision-and-Language Navigation (VLN) [2]–[4] in discrete environments [33] uses a path graph $G = \{\mathcal{V}, \mathcal{E}\}$, where $\mathcal{V} = \{V_i\}_{i=1}^N$ consists of N navigable nodes and \mathcal{E} represents the navigable edges between these nodes. The agent starts at an initial node and receives a natural language instruction $I = \{I_i\}_{i=1}^M$ containing M words. To navigate to

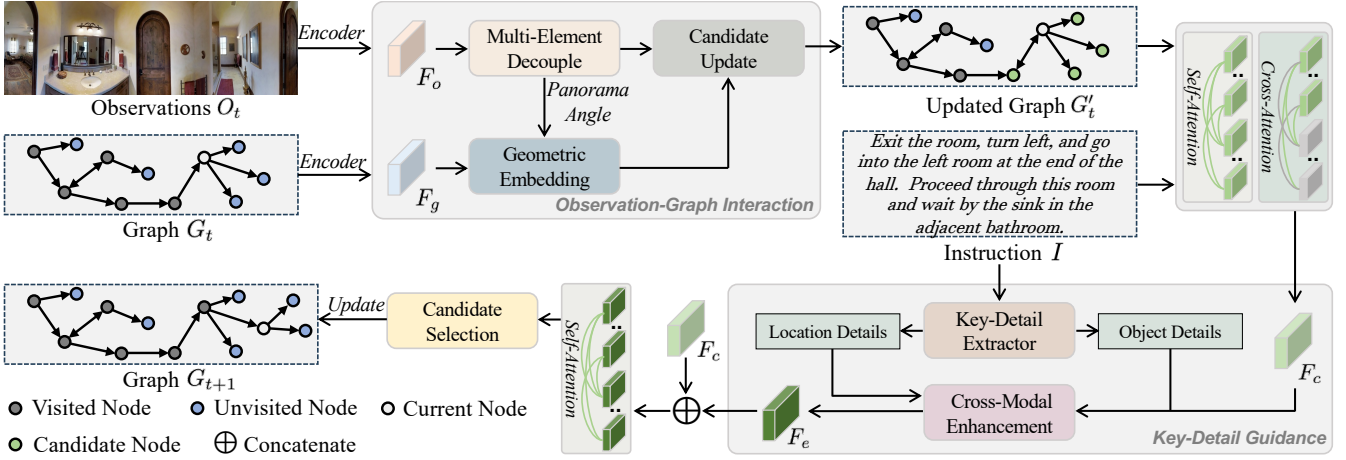


Fig. 2. Illustration of our proposed OIKG architecture. At time step t , given the observation O_t and the path graph G_t , the observation features F_o and graph features F_g are extracted respectively, where the Observation-Graph Interaction module is employed to strengthen the edge representation and update the candidate nodes. Then, we design the Key-Detail Guidance module to further extract the detailed information from the text instruction I , and enhance the alignment between instruction and navigation path. Finally, a Candidate Selection module updates the path graph G_{t+1} for the next step.

the target location, the agent should interpret this instruction while utilizing data from its RGB and depth cameras.

At each time step t , the agent at node V_t gathers information about its surroundings. The agent first observes a 360-degree panoramic view $O_t = \{r_{t,i}\}_{i=1}^K$ consisting of K different viewpoints, where $r_{t,i}$ represents the extracted image features from the i -th viewpoint. The agent also knows the available navigable nodes $\mathcal{N}(V_i)$, which are a subset of \mathcal{V} . For each neighboring node, the agent has access to its spatial coordinates and orientation relative to the current node. Guided by these observations, the agent should strategically evaluate transitioning to adjacent nodes versus maintaining its current position. Successful navigation is operationally defined as the agent achieving stabilized coordinates within a 3-meter Euclidean distance threshold from the designated target location. The system balances between following language instructions and finding target objects described by these instructions within a fixed time T , while utilizing cross-domain visual representations from the environment.

B. Model Overview

Fig. 2 illustrates the architecture of our OIKG. Initially, we extract the observation features F_o using the pre-trained visual model [11] from the panoramic observations O_t at time step t . Furthermore, previous methods [4], [8] directly utilized panoramic features to represent visited nodes in their path representation. However, this process faces a fundamental limitation: panoramic views of unvisited nodes are inherently unavailable since the agent has not physically reached those locations. Consequently, these methods have been forced to represent unvisited nodes using only directional views toward them, creating an inconsistent representation scheme between visited and unvisited nodes. To address this limitation, we propose constructing a directed graph structure $G_t = \{\mathcal{V}_t, \mathcal{E}_t\}$ that incrementally incorporates nodes and directed edges [9], [31], [34] at time step t . The directed edges

\mathcal{E}_t capture the visual observations corresponding to specific directions from each node. These edges are subsequently combined to construct the graph features F_g . It is worth noting that observation and graph features not only contain visual features, but also combine with angular information.

To facilitate deeper interaction between the observation and the graph, we propose the observation-graph interaction module (Sec. III-C). This module decouples the observation features F_o into distinct components, separately processing angular and visual information to mitigate potential interference. The panorama angle derived from the observation features is subsequently integrated with the graph features F_g through geometric embedding, thereby enriching the representation of edges. Finally, the candidate nodes are iteratively updated to generate the updated graph G'_t .

After obtaining the updated graph, the text instruction I is introduced to guide the agent toward the target location. Specifically, the graph G'_t is combined with the instruction I using a multi-layer transformer decoder [20] to get the cross-modal features F_c . We then introduce the key-detail guidance module (Sec. III-D) to dynamically extract fine-grained information from the instruction, including location and object details. Furthermore, detailed interaction is achieved through cross-modal enhancement to obtain the enhanced features F_e , enabling more precise guidance throughout the navigation process. Finally, since the enhanced candidate feature encodes the alignment between the instruction and the candidate nodes, we predict a target node and update the graph through candidate selection. This process utilizes a single-layer transformer encoder followed by an Multi-Layer Perceptron (MLP).

C. Observation-Graph Interaction

Given the observation features F_o and graph features F_g , we introduce the observation-graph interaction module to enhance edge representation and iteratively update the candidate nodes. Specifically, the observation features encom-

pass both angular and visual information. Processing these features as a unified whole can lead to mutual interference between the internal components. To address this, we first decouple the observation features, then separately embed the angular and visual information to derive angular embedding E_a and visual embedding E_v . Finally, we merge these two sets of embeddings to obtain the processed observation features F'_o :

$$F'_o = \mathcal{F}(\text{cat}[E_a, E_v]), \quad (1)$$

where $\text{cat}[\cdot]$ denotes the concatenation, $\mathcal{F}(\cdot)$ represents the fusion function, consisting of an MLP.

For graph features, we only utilize the angular information for directional perception. The angular information encompasses both the heading and elevation angles. Heading information receives prioritized consideration due to its dominant role in horizontal plane navigation decisions, in contrast to elevation angles which exhibit minimal variance under typical conditions. In terms of heading angle α , we extract the sine and cosine representations from the graph features, denoted as $\sin(\alpha)$ and $\cos(\alpha)$. At the same time, we also extract the corresponding sine and cosine representations from the observation features, expressed as $\sin(\alpha')$ and $\cos(\alpha')$. And we use the trigonometric formula to calculate the difference d in relative angles:

$$d = |(\text{atan2}[\sin(\alpha - \alpha'), \cos(\alpha - \alpha')])|. \quad (2)$$

After that, we find the angular distance d' closest to the candidate view through d , and combine it with the sine-cosine difference of the relative angle to obtain the final positional embedding pe :

$$pe = \mathcal{P}(\text{cat}[d', \sin(\alpha - \alpha'), \cos(\alpha - \alpha')]), \quad (3)$$

where $\mathcal{P}(\cdot)$ denotes the positional function and consists of a linear layer. The incorporation of positional embeddings further enables the agent to comprehend the spatial relationships between candidate nodes relative to its current position, effectively differentiating nodes in various directions. The final candidate features F'_g are obtained by combining positional embedding with the raw angular information through element-wise addition:

$$F'_g = \mathcal{C}(\text{cat}[\sin(\alpha), \cos(\alpha), \sin(\beta), \cos(\beta)]) + pe, \quad (4)$$

where β is the elevation angle and $\mathcal{C}(\cdot)$ represents the candidate function, consisting of a linear layer.

Finally, we update the directed edge features for each candidate node, resulting in an updated graph G'_t . Specifically, we employ a layer of transformer decoder [20] for interaction, wherein candidate features are utilized as the query, while observation features serve as the key and value. This process ensures that the directed edges corresponding to each candidate node in the updated graph are concentrated on specific directional regions.

Instruction	Location
Exit the bedroom , go passed the table with china on it, turn left into the doorway , and then turn right , go straight passed the china case and then turn left into the doorway. Step between the bed and the window on the right and stop.	bedroom doorway right between
	Object
	table china china case bed bed window

Fig. 3. The process of extracting location and object details from the original instruction.

D. Key-Detail Guidance

After obtaining the updated graph G'_t , instruction I is introduced to guide the agent in navigating to a specific location based on its semantics. The updated graph is first combined with the instruction using a multi-layer transformer decoder to obtain the cross-modal feature F_c . However, existing methods [4], [8], [9], [35] merely integrate instruction information through cross-attention mechanisms [20], lacking fine-grained instructional guidance and containing redundant information, which impedes effective vision-language navigation planning for embodied agents. To address this limitation, we use a large language model (LLM) [36] to sort out the text of the R2R [2] and RxR [3] datasets and summarize them into two word bases, namely location details and object details, as illustrated in Fig. 3. Then we extract the corresponding features from the text instruction based on the indices of location details and object details, and fuse them to generate key detail features F_k :

$$F_k = \mathcal{F}'(\text{cat}[\mathcal{E}_L(F_i), \mathcal{E}_O(F_i)]), \quad (5)$$

where F_i denotes the instruction features extracted by the text extractor (a multi-layer transformer encoder initialized with pretrained language models [12], [13]). $\mathcal{F}'(\cdot)$ represents the key-detail fusion function, while $\mathcal{E}_L(\cdot)$ and $\mathcal{E}_O(\cdot)$ refer to the location and object extractors, respectively, which consist of a linear layer with an activation function.

To enhance the agent’s navigation capabilities, we incorporate a specialized cross-modal enhancement module that facilitates fine-grained feature interactions. This module comprises a cross-attention mechanism coupled with a linear projection layer, where cross-modal features F_c serve as queries while key-detail features F_k as keys and values. Through the design of the architecture, the module effectively captures spatial relationships and object-centric information, producing enhanced feature F_e that are particularly attuned to navigational cues and environmental details. Finally, we aggregate the enhanced features with cross-modal features through a residual connection, followed by a self-attention mechanism to model global dependencies. An MLP processes the refined features to compute alignment scores for each candidate node, where the scores indicate the semantic correspondence between the navigation instruction and potential trajectories. The predicted action a_t^p is then made by selecting the candidate node with the maximum alignment score, and the topological graph is dynamically updated to accommodate this selection for the next time step.

TABLE I

EVALUATION RESULTS ON R2R DATASET UNDER DIFFERENT SETTINGS. BEST PERFORMANCE IS HIGHLIGHTED IN BOLD.

Methods	Val Seen				Val Unseen				Test Unseen			
	TL	NE↓	SR↑	SPL↑	TL	NE↓	SR↑	SPL↑	TL	NE↓	SR↑	SPL↑
Seq2Seq-SF [2]	11.33	6.01	39	-	8.39	7.81	22	-	8.13	7.85	28	18
Speaker-Follower [14]	-	3.36	66	-	-	6.62	35	-	14.82	6.62	35	28
RCM [15]	10.65	3.53	67	-	11.46	6.09	43	-	11.97	6.12	43	38
Regretful [37]	-	3.23	69	63	-	5.32	50	41	-	5.69	56	40
EnvDrop [17]	11.00	3.99	62	59	10.70	5.22	52	48	11.66	5.23	51	47
PREVALENT [23]	10.32	3.67	69	65	10.19	4.71	58	53	10.51	5.30	54	51
NvEM [38]	11.09	3.44	69	65	11.83	4.27	60	55	12.98	4.37	58	54
SSM [32]	14.70	3.10	71	62	20.70	4.32	62	45	20.40	4.57	61	46
RecBert [39]	11.13	2.90	72	68	12.01	3.93	63	57	12.35	4.09	63	57
HAMT [16]	11.15	2.51	76	72	11.46	2.29	66	61	12.27	3.93	65	60
MTVM [24]	-	2.67	74	69	-	3.73	66	59	-	3.85	65	59
DUET [4]	12.32	2.28	79	73	13.94	3.31	72	60	14.73	3.65	69	59
AZHP [5]	-	-	-	-	14.05	3.15	72	61	14.95	3.52	71	60
Meta-Explore [6]	11.95	2.11	81	75	13.09	3.22	72	62	14.25	3.57	71	61
GridMM [7]	-	-	-	-	13.27	2.83	75	64	14.43	3.35	73	62
BEVBert [8]	13.56	2.17	81	74	14.55	2.81	75	64	15.87	3.13	73	62
PRET [9]	11.25	2.41	78	72	11.87	2.90	74	65	12.21	3.09	72	64
OIKG(Ours)	11.58	2.18	81	76	12.37	2.68	75	65	13.40	3.05	74	64

E. Loss Function

Following established training paradigms [4], [8], [9], [23] in VLN, we first leverage Masked Language Modeling (MLM) as a pre-training objective to initialize our model. Specifically, we randomly mask 15% of the input tokens and process them through the text encoder. The encoded token, along with directed edge features, are then passed through a transformer decoder. The decoder outputs are utilized to reconstruct the masked tokens, enabling the model to learn rich cross-modal representations that effectively align textual instructions with directed edge features. This pre-training strategy significantly enhances the ability of the model to ground natural language instructions in the navigation space.

After initializing the model, we employ a hybrid learning strategy that combines teacher-forcing and student-forcing strategies for fine-tuning. During the teacher-forcing phase, the agent is trained to follow the ground-truth actions a_t^{gt} while using the model-predicted actions a_t^p . In the student-forcing stage, pseudo actions a_t' are sampled from the agent's predicted distribution to promote exploration and mitigate exposure bias. For trajectories deviated from ground-truth paths, we adopt the nearest unvisited ground-truth node as a pseudo-label to learn recovery strategies. When no unvisited ground-truth nodes are available, pseudo-labels are derived from the shortest path between current and target positions. The loss function is defined as:

$$\mathcal{L} = \lambda \left(\frac{1}{T} \sum_{t=1}^T \eta(a_t^p, a_t^{gt}) \right) + (1 - \lambda) \left(\frac{1}{T} \sum_{t=1}^T \eta(a_t^p, a_t') \right), \quad (6)$$

where λ is the weight coefficient, T is the total number of time steps and $\eta(\cdot)$ represents the cross-entropy function.

TABLE II

EVALUATION RESULTS ON RxR DATASET UNDER DIFFERENT SETTINGS. BEST PERFORMANCE IS HIGHLIGHTED IN BOLD.

Methods	Val Seen				Val Unseen			
	NE↓	SR↑	nDTW↑	sDTW↑	NE↓	SR↑	nDTW↑	sDTW↑
LSTM [3]	10.7	25.2	42.2	20.7	10.9	22.8	38.9	18.2
EnvDrop+ [40]	-	-	-	-	-	43.6	55.7	-
HAMT [16]	-	59.4	65.3	50.9	-	56.5	63.1	48.3
EnvEdit [18]	-	67.2	71.1	58.5	-	62.8	68.5	54.6
MPM [41]	-	67.7	71.0	58.9	-	63.5	67.7	54.5
MARVEL [42]	3.0	75.9	79.1	68.8	4.5	64.8	70.8	57.5
BEVBert [8]	3.2	75.0	76.3	66.7	4.0	68.5	69.6	58.6
PRET [9]	2.4	79.3	80.4	70.7	3.2	72.8	73.4	62.4
OIKG(Ours)	1.9	83.3	84.0	75.8	2.8	74.7	74.8	64.2

IV. EXPERIMENTS

A. Implementation Details

We implement and evaluate OIKG using PyTorch [43] on a single NVIDIA A6000 GPU. The models are trained with the AdamW [44] optimizer. During the pre-training stage, the learning rate is set to $2e-5$, the batch size is 16, and the number of training iterations is 100,000. In the fine-tuning stage, the learning rate is set to $1e-5$, the batch size is 8, and the number of training iterations is 200,000. The weight coefficient λ in loss function is set to 0.2. For both the R2R and RxR datasets, we utilize augmented data from previous works [23], [42].

B. Comparison on R2R Dataset

1) *R2R Dataset*: The R2R (Room-to-Room) [2] dataset contains 10,800 panoramic views (36 images per view) and

Leave the room and take a right. Walk pass the stairs and enter the bedroom on the right. Stop once you pass the door to the bedroom.



Fig. 4. Qualitative results on the R2R Dataset. The green box indicates the location details, and the blue box represents the object details.

7,189 trajectories, each paired with three instructions. The dataset spans 90 scenes and is split into train, validation seen, validation unseen, and test unseen sets. The validation seen split uses the same scenes as the training set. All paths in R2R represent the shortest routes between start and target nodes.

2) *Metrics*: Following [8], [9], we assess the performance using four metrics: (a) Trajectory Length (TL), which measures the average length of the navigation trajectory. (b) Navigation Error (NE), which indicates the mean of the shortest path distance in meters between the agent’s final location and the target location. (c) Success Rate (SR), which represents the percentage of the agent’s final location that is less than 3 meters away from the target location. (d) Success weighted by Path Length (SPL), which balances SR against TL , a higher score indicates more efficiency in navigation.

3) *Results*: We compare the quantitative results of our method with other recent methods, such as Seq2Seq-SF [2], Speaker-Follower [14], RCM [15], Regretful [37], EnvDrop [17], PREVALENT [23], NvEM [38], SSM [32], RecBert [39], HAMT [16], MTVM [24], DUET [4], AZHP [5], Meta-Explore [6], GridMM [7], BEVBert [8] and PRET [9]. The evaluation results are illustrated in Table I. In various settings, our method achieves superior performance compared to previous state-of-the-art methods, particularly on the primary metric, SPL . We also present qualitative results in Fig. 4, which demonstrate that our method can accurately follow instructions to complete navigation planning. For additional qualitative results, please view the supplementary video.

C. Comparison on RxR Dataset

1) *RxR Dataset*: RxR (Room-across-Room) [3] is a large multilingual dataset. It contains a total of 126,000 instructions, equally distributed across three languages: English, Hindi, and Telugu, with 42,000 instructions in each language. Compared to R2R, the paths in RxR are longer and do not represent the shortest possible routes. Furthermore, RxR instructions are lengthier and contain more detailed descriptions than those in R2R.

2) *Metrics*: Due to the paths in the RxR dataset being shortest paths, TL and SPL are unsuitable. Therefore, we follow previous works [8], [9] to evaluate our OIKG

TABLE III
ABLATION STUDIES OF EACH COMPONENT.

#	MED	GE	LD	OD	TL	NE↓	SR↑	SPL↑	time(ms)↓
1	-	-	-	-	12.59	3.01	73.32	63.07	3.69
2	✓	-	-	-	12.72	2.97	74.13	63.48	3.75
3	✓	✓	-	-	12.41	2.85	74.70	63.72	3.80
4	✓	✓	✓	-	12.30	2.84	74.78	64.24	3.97
5	✓	✓	✓	✓	12.37	2.68	75.54	65.60	4.08

with four metrics: (a) Navigation Error (NE). (b) Success Rate (SR). (c) Normalized Dynamic Time Warping ($nDTW$), which measures trajectory similarity between agent path and ground-truth path using Dynamic Time Warping algorithm (range [0,1]). (d) Success weighted Dynamic Time Warping ($sDTW$), which incorporates success rate (SR) as a weight into $nDTW$.

3) *Results*: We evaluate the performance of our OIKG by comparing its results with several recent methods, including LSTM [3], EnvDrop+ [40], HAMT [16], EnvEdit [18], MPM [41], MARVEL [42], BEVBert [8] and PRET [9]. Table II presents the evaluation results, demonstrating that our method achieves state-of-the-art performance across all metrics. Notably, the RxR dataset is more challenging than the R2R dataset, and the outstanding performance of our method highlights the effectiveness of its components.

D. Ablation Study

We conducted ablation experiments on various components of our OIKG, with results reported on the R2R val unseen split. As shown in Table III, all components contributed to performance improvements. The multi-element decouple (MED) module (Row 2) mitigates interference between angular and visual information. The geometric embedding (GE) module (Row 3) enhances edge representation. The addition of location details (LD) and object details (OD) (Rows 4 and 5) enables our model to dynamically extract fine-grained information from instructions, resulting in more precise navigation planning. Moreover, the addition of different components does not significantly increase the inference time.

V. CONCLUSION

In this paper, we present OIKG, a novel approach to vision-and-language navigation that combines observation-

graph interaction with key-detail guidance. The observation-graph interaction component reduces interference between angular and visual information while enhancing edge representation in the navigation space. Our key-detail guidance module dynamically extracts fine-grained information from navigation instructions, enabling more precise path planning. Extensive experimental results across multiple settings demonstrate OIKG’s superior performance compared to existing methods.

REFERENCES

- [1] J. Gu, E. Stefani, Q. Wu, J. Thomason, and X. Wang, “Vision-and-language navigation: A survey of tasks, methods, and future directions,” in *Proceedings of the 60th Annual Meeting of the Association for Computational Linguistics (Volume 1: Long Papers)*, 2022, pp. 7606–7623.
- [2] P. Anderson, Q. Wu, D. Teney, J. Bruce, M. Johnson, N. Sünderhauf, I. Reid, S. Gould, and A. Van Den Hengel, “Vision-and-language navigation: Interpreting visually-grounded navigation instructions in real environments,” in *Proceedings of the IEEE Conference on Computer Vision and Pattern Recognition*, 2018, pp. 3674–3683.
- [3] A. Ku, P. Anderson, R. Patel, E. Ie, and J. Baldrige, “Room-across-room: Multilingual vision-and-language navigation with dense spatiotemporal grounding,” in *Proceedings of the 2020 Conference on Empirical Methods in Natural Language Processing (EMNLP)*, 2020, pp. 4392–4412.
- [4] S. Chen, P.-L. Guhur, M. Tapaswi, C. Schmid, and I. Laptev, “Think global, act local: Dual-scale graph transformer for vision-and-language navigation,” in *Proceedings of the IEEE/CVF Conference on Computer Vision and Pattern Recognition*, 2022, pp. 16 537–16 547.
- [5] C. Gao, X. Peng, M. Yan, H. Wang, L. Yang, H. Ren, H. Li, and S. Liu, “Adaptive zone-aware hierarchical planner for vision-language navigation,” in *Proceedings of the IEEE/CVF Conference on Computer Vision and Pattern Recognition*, 2023, pp. 14 911–14 920.
- [6] M. Hwang, J. Jeong, M. Kim, Y. Oh, and S. Oh, “Meta-explore: Exploratory hierarchical vision-and-language navigation using scene object spectrum grounding,” in *Proceedings of the IEEE/CVF Conference on Computer Vision and Pattern Recognition*, 2023, pp. 6683–6693.
- [7] Z. Wang, X. Li, J. Yang, Y. Liu, and S. Jiang, “Gridmm: Grid memory map for vision-and-language navigation,” in *Proceedings of the IEEE/CVF International Conference on Computer Vision*, 2023, pp. 15 625–15 636.
- [8] D. An, Y. Qi, Y. Li, Y. Huang, L. Wang, T. Tan, and J. Shao, “Bevbert: Multimodal map pre-training for language-guided navigation,” in *Proceedings of the IEEE/CVF International Conference on Computer Vision*, 2023, pp. 2737–2748.
- [9] R. Lu, J. Meng, and W.-S. Zheng, “Pret: Planning with directed fidelity trajectory for vision and language navigation,” in *European Conference on Computer Vision*. Springer, 2024, pp. 72–88.
- [10] A. Radford, J. W. Kim, C. Hallacy, A. Ramesh, G. Goh, S. Agarwal, G. Sastry, A. Askell, P. Mishkin, J. Clark *et al.*, “Learning transferable visual models from natural language supervision,” in *International conference on machine learning*. PMLR, 2021, pp. 8748–8763.
- [11] M. Oquab, T. Darcet, T. Moutakanni, H. Vo, M. Szafraniec, V. Khalidov, P. Fernandez, D. Haziza, F. Massa, A. El-Nouby *et al.*, “Dinov2: Learning robust visual features without supervision,” *Transactions on Machine Learning Research Journal*, pp. 1–31, 2024.
- [12] J. Li, R. Selvaraju, A. Gotmare, S. Joty, C. Xiong, and S. C. H. Hoi, “Align before fuse: Vision and language representation learning with momentum distillation,” *Advances in Neural Information Processing Systems*, vol. 34, pp. 9694–9705, 2021.
- [13] A. Conneau, “Unsupervised cross-lingual representation learning at scale,” *arXiv preprint arXiv:1911.02116*, 2019.
- [14] D. Fried, R. Hu, V. Cirik, A. Rohrbach, J. Andreas, L.-P. Morency, T. Berg-Kirkpatrick, K. Saenko, D. Klein, and T. Darrell, “Speaker-follower models for vision-and-language navigation,” *Advances in neural information processing systems*, vol. 31, 2018.
- [15] X. Wang, Q. Huang, A. Celikyilmaz, J. Gao, D. Shen, Y.-F. Wang, W. Y. Wang, and L. Zhang, “Reinforced cross-modal matching and self-supervised imitation learning for vision-language navigation,” in *Proceedings of the IEEE/CVF conference on computer vision and pattern recognition*, 2019, pp. 6629–6638.
- [16] S. Chen, P.-L. Guhur, C. Schmid, and I. Laptev, “History aware multimodal transformer for vision-and-language navigation,” *Advances in neural information processing systems*, vol. 34, pp. 5834–5847, 2021.
- [17] H. Tan, L. Yu, and M. Bansal, “Learning to navigate unseen environments: Back translation with environmental dropout,” in *Proceedings of the 2019 Conference of the North American Chapter of the Association for Computational Linguistics: Human Language Technologies, Volume 1 (Long and Short Papers)*, 2019, pp. 2610–2621.
- [18] J. Li, H. Tan, and M. Bansal, “Envedit: Environment editing for vision-and-language navigation,” in *Proceedings of the IEEE/CVF Conference on Computer Vision and Pattern Recognition*, 2022, pp. 15 407–15 417.
- [19] C. Liu, F. Zhu, X. Chang, X. Liang, Z. Ge, and Y.-D. Shen, “Vision-language navigation with random environmental mixup,” in *Proceedings of the IEEE/CVF International Conference on Computer Vision*, 2021, pp. 1644–1654.
- [20] A. Vaswani, “Attention is all you need,” *Advances in Neural Information Processing Systems*, 2017.
- [21] Y. Xie, J. Zhu, S. Li, and P. Shi, “Cross-modal information-guided network using contrastive learning for point cloud registration,” *IEEE Robotics and Automation Letters*, vol. 9, no. 1, pp. 103–110, 2023.
- [22] Y. Xie, T. Feng, X. Zhang, X. Luo, Z. Guo, W. Yu, H. Chang, F. Ma, and F. R. Yu, “Pointtalk: Audio-driven dynamic lip point cloud for 3d gaussian-based talking head synthesis,” *arXiv preprint arXiv:2412.08504*, 2024.
- [23] W. Hao, C. Li, X. Li, L. Carin, and J. Gao, “Towards learning a generic agent for vision-and-language navigation via pre-training,” in *Proceedings of the IEEE/CVF Conference on Computer Vision and Pattern Recognition*, 2020, pp. 13 137–13 146.
- [24] C. Lin, Y. Jiang, J. Cai, L. Qu, G. Haffari, and Z. Yuan, “Multimodal transformer with variable-length memory for vision-and-language navigation,” in *European Conference on Computer Vision*. Springer, 2022, pp. 380–397.
- [25] J. Fuentes-Pacheco, J. Ruiz-Ascencio, and J. M. Rendón-Mancha, “Visual simultaneous localization and mapping: a survey,” *Artificial intelligence review*, vol. 43, pp. 55–81, 2015.
- [26] Y. Wang, Y. Tian, J. Chen, K. Xu, and X. Ding, “A survey of visual slam in dynamic environment: the evolution from geometric to semantic approaches,” *IEEE Transactions on Instrumentation and Measurement*, 2024.
- [27] J. F. Henriques and A. Vedaldi, “Mapnet: An allocentric spatial memory for mapping environments,” in *proceedings of the IEEE Conference on Computer Vision and Pattern Recognition*, 2018, pp. 8476–8484.
- [28] Y. Xie, J. Zhu, S. Li, N. Hu, and P. Shi, “Hecpg: Hyperbolic embedding and confident patch-guided network for point cloud matching,” *IEEE Transactions on Geoscience and Remote Sensing*, 2024.
- [29] D. S. Chaplot, D. P. Gandhi, A. Gupta, and R. R. Salakhutdinov, “Object goal navigation using goal-oriented semantic exploration,” *Advances in Neural Information Processing Systems*, vol. 33, pp. 4247–4258, 2020.
- [30] D. S. Chaplot, R. Salakhutdinov, A. Gupta, and S. Gupta, “Neural topological slam for visual navigation,” in *Proceedings of the IEEE/CVF conference on computer vision and pattern recognition*, 2020, pp. 12 875–12 884.
- [31] K. Chen, J. K. Chen, J. Chuang, M. Vázquez, and S. Savarese, “Topological planning with transformers for vision-and-language navigation,” in *Proceedings of the IEEE/CVF Conference on Computer Vision and Pattern Recognition*, 2021, pp. 11 276–11 286.
- [32] H. Wang, W. Wang, W. Liang, C. Xiong, and J. Shen, “Structured scene memory for vision-language navigation,” in *Proceedings of the IEEE/CVF conference on Computer Vision and Pattern Recognition*, 2021, pp. 8455–8464.
- [33] A. Chang, A. Dai, T. Funkhouser, M. Halber, M. Niebner, M. Savva, S. Song, A. Zeng, and Y. Zhang, “Matterport3d: Learning from rgb-d data in indoor environments,” in *International Conference on 3D Vision (3DV)*, 2017.
- [34] D. Rawlinson and R. Jarvis, “Topologically-directed navigation,” *Robotica*, vol. 26, no. 2, pp. 189–203, 2008.
- [35] D. An, H. Wang, W. Wang, Z. Wang, Y. Huang, K. He, and L. Wang, “Etpnav: Evolving topological planning for vision-language navigation

- in continuous environments,” *IEEE Transactions on Pattern Analysis and Machine Intelligence*, 2024.
- [36] H. Touvron, T. Lavril, G. Izacard, X. Martinet, M.-A. Lachaux, T. Lacroix, B. Rozière, N. Goyal, E. Hambro, F. Azhar *et al.*, “Llama: Open and efficient foundation language models,” *arXiv preprint arXiv:2302.13971*, 2023.
- [37] C.-Y. Ma, Z. Wu, G. AlRegib, C. Xiong, and Z. Kira, “The regretful agent: Heuristic-aided navigation through progress estimation,” in *Proceedings of the IEEE/CVF conference on Computer Vision and Pattern Recognition*, 2019, pp. 6732–6740.
- [38] D. An, Y. Qi, Y. Huang, Q. Wu, L. Wang, and T. Tan, “Neighbor-view enhanced model for vision and language navigation,” in *Proceedings of the 29th ACM International Conference on Multimedia*, 2021, pp. 5101–5109.
- [39] Y. Hong, Q. Wu, Y. Qi, C. Rodriguez-Opazo, and S. Gould, “Vln bert: A recurrent vision-and-language bert for navigation,” in *Proceedings of the IEEE/CVF conference on Computer Vision and Pattern Recognition*, 2021, pp. 1643–1653.
- [40] S. Shen, L. H. Li, H. Tan, M. Bansal, A. Rohrbach, K.-W. Chang, Z. Yao, and K. Keutzer, “How much can clip benefit vision-and-language tasks?” in *International Conference on Learning Representations*.
- [41] Z.-Y. Dou, F. Gao, and N. Peng, “Masked path modeling for vision-and-language navigation,” in *The 2023 Conference on Empirical Methods in Natural Language Processing*.
- [42] S. Wang, C. Montgomery, J. Orbay, V. Birodkar, A. Faust, I. Gur, N. Jaques, A. Waters, J. Baldrige, and P. Anderson, “Less is more: Generating grounded navigation instructions from landmarks,” in *Proceedings of the IEEE/CVF Conference on Computer Vision and Pattern Recognition*, 2022, pp. 15 428–15 438.
- [43] A. Paszke, S. Gross, F. Massa, A. Lerer, J. Bradbury, G. Chanan, T. Killeen, Z. Lin, N. Gimelshein, L. Antiga *et al.*, “Pytorch: An imperative style, high-performance deep learning library,” *Advances in Neural Information Processing Systems*, vol. 32, 2019.
- [44] I. Loshchilov, “Decoupled weight decay regularization,” *arXiv preprint arXiv:1711.05101*, 2017.